Coordination of E–C bonds (E = Zn, Mg, Al) and the Zn–H Bonds of $(C_5Me_5)ZnH$ and $(C_5Me_5)ZnZnH$ across a Quadruply Bonded Dimolybdenum Dihydride Complex.

Marina Pérez-Jiménez,[a] Jesús Campos,[a] Jesús Jover,[b] Santiago Álvarez*,[b] Ernesto Carmona*[a]

[a] Instituto de Investigaciones Químicas (IIQ), Departamento de Química Inorgánica and Centro de Innovación en Química Avanzada (ORFEO-CINQA), Consejo Superior de Investigaciones Científicas (CSIC) and University of Sevilla, Avda. Américo Vespucio, 49, 41092 Sevilla, Spain.

[b] Department de Química Inorgànica I Orgànica, Secció de Química Inorgànica, and Institut de Química Teòrica i Computacional Universitat de Barcelona Martí i Franquès 1-11, 08028 Barcelona, Spain.

Supporting Information Placeholder

ABSTRACT: Heterobimetallic complexes containing M–C–E linkages (M = transition metal atom; E = main group metal) have been postulated as relevant intermediates in cross-coupling reactions. Despite this, structural data for these species are scarce. In this contribution we explore the coordination of E–C bonds (E = Zn, Mg, Al) to the Mo atoms of dimolybdenum complexes containing quadruple Mo–Mo bonds. Besides, the reactivity of the bis(hydride) $[Mo_2(H)_2(\mu\text{-}Ad^{Dipp2})_2(thf)_2]$ complex (Ad^{Dipp2} = $HC[N(2,6\text{-}{}^{i}Pr_2C_6H_3)]_2$) with the zincocenes $Zn(C_5Me_5)_2$ and $Zn_2(\eta^5\text{-}C_5Me_5)_2$ reveals the formation of new dimolybdenum compounds in which $(C_5Me_5)Zn$–H and $(C_5Me_5)ZnZn$–H bonds bind to the *trans*-H–Mo≣Mo–H core. DFT calculations and an NBO analysis disclose a general bonding mechanism for the reported H–Mo≣Mo–E-R rings that is consistent with the penetration indices of the different atom pairs. The bonding comprises 3 center-2 electron Mo-H-E and Mo-R-E bonds supplemented by π-coordination of the Mo≣Mo bond to the electropositive metal E.

INTRODUCTION

In the last decades, intense efforts have been devoted to the study of transition metal complexes containing coordinated main-group metal E–H bonds, particularly those of Mg, Al or Zn.[1] This research was propelled, in no little part, by the capacity of heterobimetallic species containing M–H–E (M = transition metal) cores as intermediates in catalytic processes.[2] Similarly, coordinating electropositive main group species with E–C bonds to transition metal catalysts was very early recognized and exploited for catalytic purposes when seeking an understanding of the 'nickel effect'.[3] Besides, the use of main group organometallics, particularly those based on magnesium, zinc and to a lesser extent aluminum, is generalized in transition metal catalyzed cross-coupling processes.[4] Structures constructed around M–C–E motifs have been amply postulated as key intermediates in these transformations.[5] On these grounds, it seems surprising that information on transition metal σ-E–C complexes is yet rather scarce compared to their σ E–H analogs. For instance, the first examples of coordinated Mg–C bonds to transition metal centers were reported in the 1980s as a result of the pioneering work of Wilke and coworkers.[6] The X-ray structure analysis of $[(tmeda)Mg(CH_3)(\mu\text{-}CH_3)Ni(C_2H_4)_2]$ showed a $Ni(C_2H_4)_2$ unit linked to a $(tmeda)Mg(CH_3)_2$ fragment with one bridging Mg–C bond exhibiting a distance of 2.29 Å, longer than the terminal Mg–CH_3 bond (2.15 Å).[6a] A Co complex was also prepared,[6b] viz $\{(\eta^5\text{-}C_5H_5)Co(C_2H_4)[(tmeda)Mg(C_6H_5)(Br)]\}$, from the reaction of $(\eta^5\text{-}C_5H_5)Co(C_2H_4)_2$ with $Mg(C_6H_5)Br$, featuring a phenyl group σ bonded to the cobalt atom. Some years later, other researchers provided additional examples of complexes with 3c-2e M–C–E bonds, including the V–Mg imido complex $\{[\eta^5\text{-}C_5H_5)V(NDipp)(\mu\text{-}CH_3)_2]_2Mg\}$[7], as well as magnesium aryl cuprates.[8] Relevant to polymerization catalysis, a Ti(IV) complex with a $Ti(\mu\text{-}CH_3)_2AlMe_2$ fragment that mimics the postulated resting-state during methylaluminoxane (MAO) promoted catalysis was more recently reported.[9] Besides, two Ni-based examples that contain Ni–C–Al bonds that parallel the proposed intermediates responsible for the 'nickel effect' have also been disclosed.[10]

By contrast, not few complexes that feature an E(μ-CH_3)$_2$Li (E = Mg, Zn, Al) are known, some of them with synthetic applications as metallating "ate" reagents.[11] Zinc organyls are likely the main group organometallics with wider implications in catalysis. A Ni(0)-$ZnMe_2$ derivative was investigated computationally by Montgomery *et al.* and proved to be of interest as a possible intermediate for the Ni coupling catalysis of enones, alkynes and organozinc compounds.[12] Despite the numerous studies on palladium cross-coupling reactions,[13] an X-ray search at the CSD revealed the lack of structures containing transition metal M–C–Zn bonds. However, the formation of direct Pd–Zn bonds has been demonstrated[14] and computational studies on the mechanism of the Negishi reaction have disclosed that the Zn–C bonds of Zn(CH_3)$_2$ can act as a Lewis base towards Pd(II) during the Zn(CH_3)$_2$ catalyzed isomerization of Pd(II) complexes and in transmetalation reactions.[15]

Our group has lately investigated the coordination of Li–H and Li–C bonds to Mo atoms in the dimolybdenum complex [Mo_2(H)$_2$(μ-Ad^{Dipp2})$_2$(thf)$_2$] (**1**) (Ad^{Dipp2} = HC[N(2,6-^{i}Pr$_2$C$_6$H$_3$)]$_2$), that contain a Mo–Mo quadruple bond.[16] The stabilization of these unusual structural motifs was achieved taking profit of the bifunctional Lewis acid/Lewis base behavior of the *trans*-Mo_2H_2 core (Figure 1).[17] Thus, the strong *trans*-influence of the hydride ligand imparts high electrophilicity to the Mo atoms, thanks to the availability of an empty coordination site, while the polar $Mo^{\delta+}$–$H^{\delta-}$ bonds offer a nucleophilic hydride amenable to provide stabilization to the incoming main group substrate by an overall push-pull bonding scheme.[18] We postulate that the same type of stabilization could be attained to access complexes incorporating E–C (E = Zn, Al, Mg) bonds to the coordination sphere of the (H)Mo≡Mo(H) core of compound **1**. With this aim, we investigate herein the reactions of complex **1** towards zinc organyls ($ZnMe_2$, $ZnEt_2$ and $ZnPh_2$) as well as magnesium and aluminum organometallics ($MgMe_2$ and $AlMe_3$). In addition, we have studied the behavior of cyclopentadienyl zinc reagents ($ZnCp^*_2$ and $Zn_2Cp^*_2$) for which unstable zinc hydride derivatives were unexpectedly isolated. The new species have been analyzed experimentally by X-ray diffraction studies and NMR spectroscopy, and computationally by DFT calculations. The half-arrow formalism proposed by Green, Green, and Parkin to describe three-center-two-electron (3c–2e) interactions have been employed along this contribution to represent the multicenter bonding scheme around the Mo—H and E—C bonds (E = Mg, Al, Zn).[19]

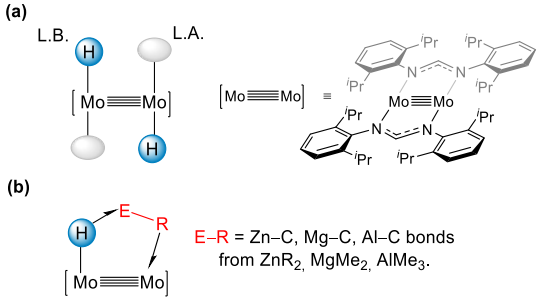

Figure 1. (a) Schematic representation of the molecular structure of complex **1,** [Mo_2(H)$_2$(μ-Ad^{Dipp2})$_2$(thf)$_2$], highlighting its Lewis acid (L.A.)/Lewis base (L.B.) behavior. **(b)** Coordination of E–R bonds to the dimolybdenum core (E = Zn, Mg, Al).

RESULTS AND DISCUSSION

Synthesis and characterization of new Mo≡Mo complexes containing coordinated E–C bonds (E = Zn, Mg, Al).

Addition of a toluene solution of complex **1** to a hexane solution of Zn(CH_3)$_2$ (1:2 molar ratio) induced a color change from red to yellow and resulted in complete consumption in a few minutes of the starting hydride, which converted into the new complex **2** (Scheme 1a) that was isolated as a yellow solid. Evaporation of the toluene followed by pentane washing afforded a pure product although crystals suitable for X-ray diffraction studies could not be obtained. Zn(CH_2CH_3)$_2$ reacted similarly providing the analogous complex **3** in the form of yellow crystals. The ^{1}H NMR spectrum in C_6D_6 at room temperature of both new products revealed a high molecular symmetry, inferred from the observation of two septets and four doublets for the methine and methyl protons of the Ad^{Dipp2} *iso*-propyl substituents. For complex **2**, there are two singlets with relative intensity 3H:3H at -0.46 and 0.32 ppm, that can be assigned to the bridging Mo–CH_3–Zn and terminal Zn–CH_3 protons, which have corresponding ^{13}C{^{1}H} resonances at 3.0 (Mo–CH_3–Zn) and -5.4 ppm (terminal Zn–CH_3). Besides, there is a singlet at 5.54 pm (2H) corresponding to the bridging hydrides of the two equivalent Mo–H–Zn linkages. For complex **3** the Mo–H–Zn bridging hydrides resonate at 5.46 ppm.

Scheme 1. a) Reactions of complex 1 with $ZnCH_2R$ to generate complexes 2 (R = H) and 3 (R = CH_3); b) Formation of the Zn(C_6H_5)$_2$ complex 4.

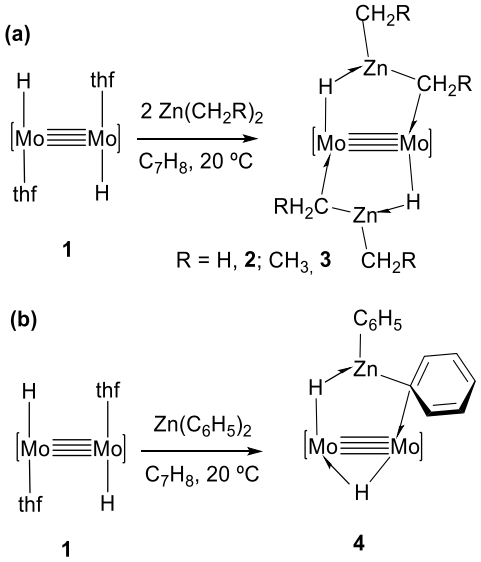

By contrast, Zn(C_6H_5)$_2$ forms a mono-adduct complex, **4** even when a 1:2 (**1**:Zn(C_6H_5)$_2$) ratio was used. In addition to the H–Mo–Mo–C–Zn metallacycle, the new complex features a Mo–H–Mo bridging moiety. The lower symmetry (four septets and eight doublets for the amidinate ligands) revealed by the ^{1}H NMR spectrum supports the formulation

as a mono-adduct complex. Furthermore, the NMR data are consistent with the existence of two different hydrides at 3.87 (Mo–H–Mo) and 7.32 ppm (Mo–H–Zn). To avoid partial overlap of the former with the amidinate *iso*-propyl septets, they are best observed at 45 ºC. These resonances show up as doublets with $^{2}J_{HH}$ = 4 Hz. In the $^{13}C\{^{1}H\}$ NMR spectrum a signal at 160.1 ppm can be assigned to the bridging *ipso* carbon, Zn–C_{ipso}–Mo, shifted by *ca*. 11 ppm to higher frequency in comparison with free $Zn(C_6H_5)_2$ (149.2 ppm in C_7D_8[20]). The three zinc hydrocarbyls employed, ZnR_2 (R = CH_3, CH_2CH_3, C_6H_5), behave similarly to their LiR counterparts recently reported by our group.[16b] For R = CH_3 and CH_2CH_3 bis-adducts are obtained while for the bulkier C_6H_5 fragment only one ZnR_2 or LiR molecule becomes coordinated to the (H)Mo≡Mo(H) core. We attributed this dissimilar reactivity to the higher steric demands of the phenyl substituents compared to methyl and ethyl analogues, a rationalization that equally applies to the present case.

The solid-state molecular structures of complexes **3** and **4** have been determined by X-ray crystallographic studies confirming the solution structures inferred from the NMR data (Figures 2a and 2b). Complex **3** can be described as a paddle-wheel structure generated by the coordination of two monoanionic *trans*-Ad^{Dipp2} and two *trans*-[(H)Zn(Et)(CH_2CH_3)] ligands. The latter are formed by coordination of two σ Zn–CH_2CH_3 bonds to the unsaturated central (H)Mo≡Mo(H) unit, intramolecularly supported by electronic interactions with the proximal, strongly polarized $Mo^{\delta+}$–$H^{\delta-}$ bonds. Within a Zn(μ-CH_2CH_3)Mo bridge portion, the Mo–CH_2 and Zn–CH_2 bond lengths are 2.29(2) and 2.31(1) Å, and the Mo–CH_2–Zn bond angle is acute, with an amplitude of 73°. The said Mo–CH_2 distance is practically identical to the corresponding distance in [Mo_2{μ-HLi(thf)CH_2CH_3}$_2$(μ-Ad^{Dipp2})$_2$],[16b] while the Zn–CH_2 distance is significantly longer than the Li–CH_2 separation in the ethyllithium complex (*ca*. 2.12 Å), and also than the 1.98(2) Å found for the terminal Zn–CH_2CH_3 bond. For comparison, the sum of the covalent radii of the atoms[21] are 2.30 and 1.98 Å, for the Mo–C and Zn–C bond, respectively. These data indicate the existence of a strong electronic interaction between the Lewis basic Zn–CH_2CH_3 bond and the Lewis acidic molybdenum atom. The two bridging hydrides in the molecules of complex **3** were located in the Fourier map and refined freely, leading to similar Mo–H and Zn–H distances of *ca*. 1.7 and 1.6 Å, respectively. On coordination, $Zn(CH_2CH_3)_2$ loses linearity as the zinc atom becomes three-coordinate, so that in complex **3** the C–Zn–C bond angle decreases to *ca*. 110°. Furthermore, the bent C–Zn–C unit is strictly coplanar with the $Mo_2Zn(C)(H)$ plane. The two Zn···Mo contacts are 2.741(2) Å for the Zn–C–Mo portion, and 2.839(2) Å within the Zn–H–Mo part, substantially shorter than the Li···Mo separations found in the bis(ethyllithium) complex.[16b] By analogy with previous studies,[16] to analyze the intermetallic bonding in complex **3** and the following, the formal shortness ratio (FSR) has been used, employing the covalent radii of the atoms. A FSR value of 0.99 was found for the Mo^{C}–Zn distance. The relatively long Mo–Mo distance of 2.163(1) Å found for complex **3** (FSR = 0.70), to be compared, for instance, with the 2.0894(1) Å value that characterizes the bis(hydride) **1** (FSR = 0.68)[22] might indicate direct donor-acceptor electronic interactions between the quadruple Mo–Mo and the electrophilic Zn atom, which is supported by the computational results.

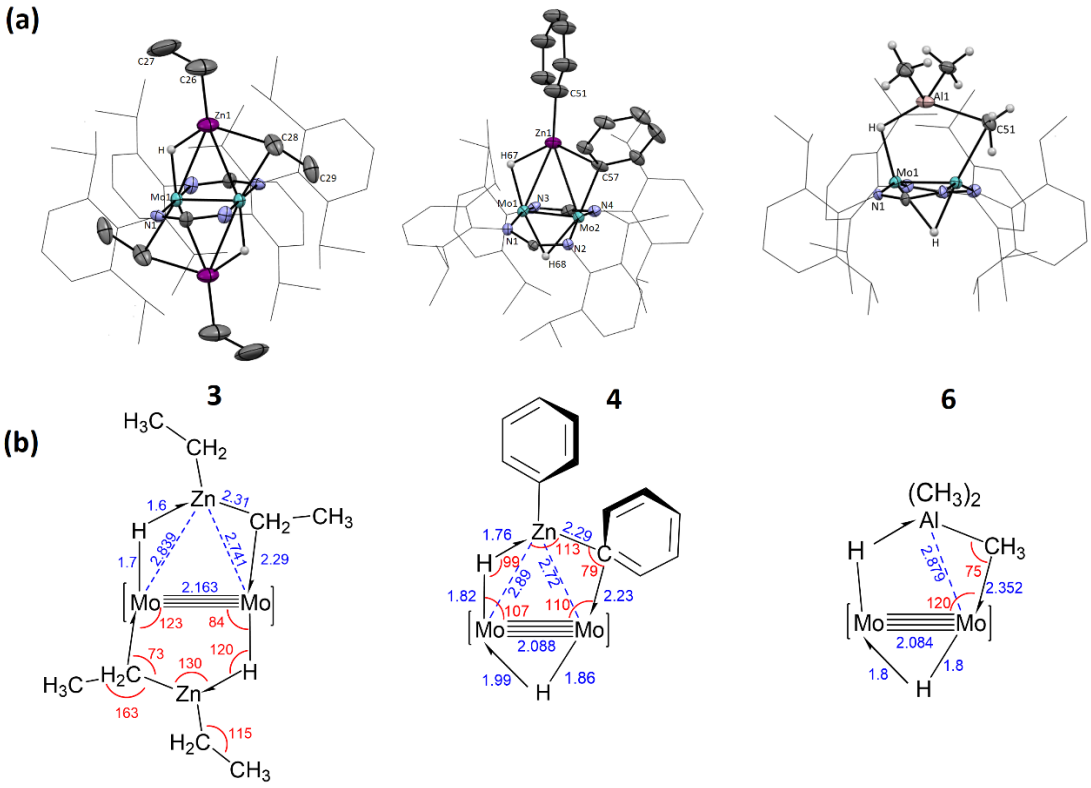

Figure 2. (a) ORTEP representations of complexes **3**, **4** and **6**. (b) Selected bond lengths (in Å) and angles (in °) of complexes **3**, **4** and **6**.

For diphenylzinc, the incorporation of only one molecule of diphenylzinc to the (H)Mo≡Mo(H) moiety results in one five membered chelating ring complemented by a 3c-2e Mo–H⟶Mo bond.[19] Besides, steric hindrance causes noticeable distortions of the paddle-wheel type structure with significant deviation from planarity of the Mo_2ZnC_{ipso} skeleton, and N–Mo–Zn and N–Mo–N bond angles of *ca*. 85 and 165°, respectively. The Zn···Mo separation along the Zn–C–Mo fragment of 2.7229(8) Å is comparable to the distance in **3**. Compared to the terminal Zn–C_6H_5 bond length of 1.97 Å, the bridging Zn–C_6H_5 is *ca.* 0.30 Å longer (Figure 2).

For $Mg(CH_3)_2$ and $Al(CH_3)_3$, the equimolar reaction with **1** affords two mono-adducts **5** and **6** (Scheme 2), respectively, where only one molecule binds to the dimolybdenum framework. At variance with $LiCH_3$ and $Zn(CH_3)_2$, addition of two equivalents of the corresponding organometallic reagents did not permit the incorporation of a second fragment of $E(CH_3)_n$. Once more we attribute this observation to steric reasons based on the higher size of Mg compared to Li and Zn,[21] and the increased steric pressure exerted by the trisubstituted Al center. The formulation proposed for complex **5** is coherent with the ^{1}H and ^{13}C{^{1}H} NMR experiments performed. In the ^{1}H NMR spectrum two different hydrides were observed: the bridging Mo–H–Mo and Mo–H–Mg hydrides, that appear as doublets with δ 3.12 and 5.24 ppm, respectively, and $^2J_{HH}$ = 6.6 Hz. In the ^{13}C{^{1}H} NMR spectrum two different signals for the terminal (-9.4 ppm) and bridging (2.8 ppm) methyl groups were detected exhibiting deshielded values compared to free $Mg(CH_3)_2$.[23] Notwithstanding its meagre thermal stability, complex **5** has been isolated in microanalytically pure form. Unfortunately, despite our efforts single-crystals suitable for X-ray studies could not be obtained. Solutions of **5** decompose at room temperature over a period of 2-3 hours, probably by binuclear reductive coupling, as hinted by the generation of CH_4 (detected by ^{1}H NMR).

Scheme 2. Synthesis of the $Mg(CH_3)_2$ and $Al(CH_3)_3$ complexes 5 and 6.

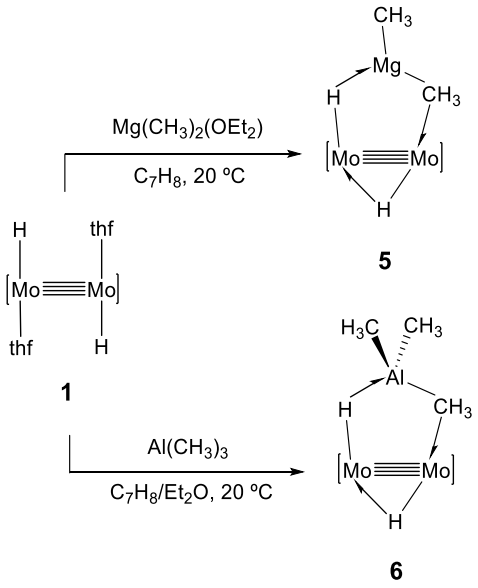

The mono-adduct **6** (Scheme 2) could be isolated as an orange crystalline solid in yields close to 60 %. In the ^{1}H NMR spectrum the metallacyclic Mo–H–$Al(CH_3)_2$–CH_3–Mo ring gives rise to two low-frequency signals at -0.11 and 0.14 ppm that correspond to the bridging and terminal Al–CH_3 groups, respectively. Two doublets, each with relative intensity corresponding to 1H and a $^2J_{HH}$ coupling of 10 Hz, are recorded at 3.04 (Mo–H–Mo) and 5.64 ppm (Mo–H–Al). The ^{13}C{^{1}H} NMR spectrum contains signals at -2.6 and 11.3 ppm due, respectively, to the terminal and bridging Al–CH_3 groups. Its molecular structure was further confirmed by X-ray crystallography (Figure 2). The Mo···Al interaction (2.879 Å in complex **6**, with FSR value of 1.05) is weaker compared to the previous Mo···Zn contact, and similar to the Ni···Al interaction in the reported Ni(II)/$Al(CH_3)_3$ compound.[10a]

Reactions of 1 with the zincocenes $Zn(C_5Me_5)_2$ and $Zn_2(\eta^5\text{-}C_5Me_5)_2$

The reactivity of **1** against zincocenes $Zn(C_5Me_5)_2$ and $Zn_2(\eta^5\text{-}C_5Me_5)_2$ resulted in the incorporation of molecular zinc hydrides [(C_5Me_5)Zn(H)] and [$(\eta^5\text{-}C_5Me_5)$Zn–Zn(H)] to the coordination sphere of the quadruple Mo–Mo bond yielding complexes **7** and **8**, respectively (Scheme 3). [(C_5Me_5)Zn(H)] has been proposed by Fischer as an unstable intermediate for an alternative synthesis of $Zn_2(\eta^5\text{-}C_5Me_5)_2$[24] from $Zn(C_5Me_5)_2$ and ZnH_2.[25] Independent work by Stephan *et al*. allowed stabilization of the hydride by coordination to zinc of the NHC ligand 1,3-bis(2,4,6-trimethylphenyl)-4,5-dihydroimidazol-2-ylidene, SIMes, in the complex [$(\eta^3\text{-}C_5Me_5)$Zn(H)(SIMes)], that was characterized by X-ray crystallography.[26] However, as far as we know the zinc-zinc bonded hydride [$(\eta^5\text{-}C_5Me_5)Zn_2$(H)] seems to be unprecedented.

Although no reaction occurs between **1** and the monozincocene in toluene at room temperature, heating at 60 °C dur-

ing 8 hours afforded a dark brown solution from which yellow crystals of complex **7** were obtained after removal of the toluene under vacuum, followed by extraction in diethyl ether and crystallization. The final product was characterized by NMR and X-ray diffraction studies. By NMR monitoring we observed the formation of C_5Me_5H and other undetermined products. The formation of C_5Me_5H was not unexpected as it has already been observed in reactions of zinc organometallics with transition metal hydrides.[27] However, no signals attributable to tetramethylfulvene, $C_6Me_4H_2$, and decamethylfulvalene, $C_{10}Me_{10}$, were detected, hinting at no participation of C_5Me_5· radicals[28] and suggesting that the source of the hydrogen atoms required for the formation of the final product could be the bis(hydride) precursor **1** itself. In fact, the overall spectroscopic yield for this transformation remained in all cases below 50%. However, by employing an external source of H atoms (H_2 atmosphere) we were able to isolate the same species in a preparative scale (see experimental section). The room temperature ^{1}H NMR spectrum of yellow crystals of **7** dissolved in C_6D_6 exhibit a singlet at 2.33 ppm with relative intensity corresponding to 15H, which indicates the presence of a fluxional, zinc-bonded $\eta^1(\pi)$-C_5Me_5 ligand, even at lower temperatures.[27] The latter originates $^{13}C\{^1H\}$ signals at 12.8 ($C_5(\mathit{C}H_3)_5$) and 115.5 ppm (C_5Me_5). Besides, two key ^{1}H NMR resonances are recorded at 3.28 and 5.19 ppm, each with relative intensity 1H:1H. The first is a broad triplet, while the second is a well-defined doublet (2H, $^2J_{HH}$ = 4.0 Hz). These signals are assigned respectively to the Mo–H–Mo and Mo–H–Zn bridges and present chemical shifts similar to those ascertained for dimolybdenum hydrides[22] and zinc hydrides.[29]

Scheme 3. Reactions of complex 1 with $Zn(C_5Me_5)_2$ and $Zn_2(C_5Me_5)_2$ to form products 7 and 8.

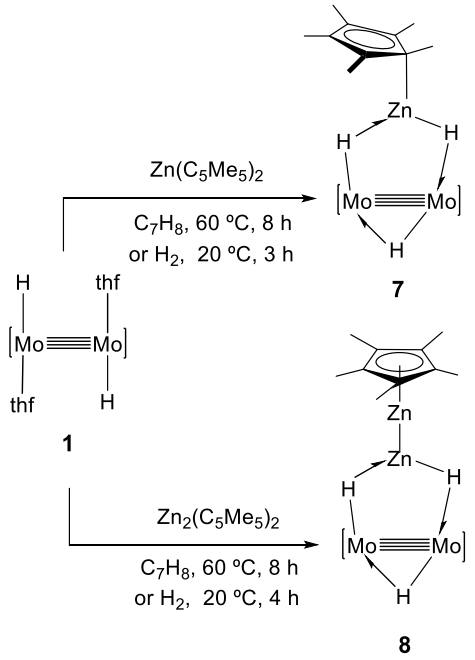

7 **1** **8**

Suitable crystals for X-ray diffraction studies were obtained for complex **7** (Figure 3). A quadruple Mo–Mo bond of length 2.080(2) Å is coordinated to two *trans* amidinate ligands, that are forced to bend by reason of the steric pressure exerted by the $Zn(C_5Me_5)$ terminus of the $(\mu\text{-}H)_2Zn(C_5Me_5)$ chelate ligand. Located on a perpendicular plane, this group causes the N–Mo–N bond angles to shrink to *ca*. 164°. Two zinc-bonded hydrogen atoms, namely H66 and H67, and the dimolybdenum bound H65, complete the coordination of the Mo≡Mo bond. The three hydrides were located in the electron density map providing longer Zn–H distances than the *ca*. 1.5 Å average value found for the terminal Zn–H[29b] and typical values for the Mo–H bonds.[22] For the Zn–$\eta^1(\pi)$Cp* units, the Zn–C distance in **7** of 2.02 Å is rather long, and the angle formed by this bond and the plane of the ring, measured as the $ZnC_{ring}C_5Me_{5(centr)}$ angle, is 101°. Besides, the Zn–C51–C bond angles involving the adjacent carbon atoms are *ca*. 98°, far from the values expected for a tetrahedral C51 atom. All these data reinforce the indicated $\eta^1(\pi)$-(C_5Me_5) coordination.[26,27] The Mo···Zn contacts of *ca*. 2.74 and 2.79 Å, along with the even shorter Zn–Mo_2(centroid) distance of 2.57 Å, clearly reveal substantial donor-acceptor interactions between the Mo≡Mo bond and the electrophilic Zn(II) atom (see NBO analysis section below). Although the molecular structure of **7** finds no literature precedent, a few examples of complexes featuring M–H–Zn bonds within metal-metal bonded dinuclear skeletons have been reported. The metallic cores of those complexes contain $Rh_2(\mu\text{-}H)_2(\mu\text{-}ZnC_5H_5)_2$,[30] $Mn_2Zn(\mu\text{-}H)_2$[31] and $V(\mu\text{-}H)_2Zn$[32] frameworks.

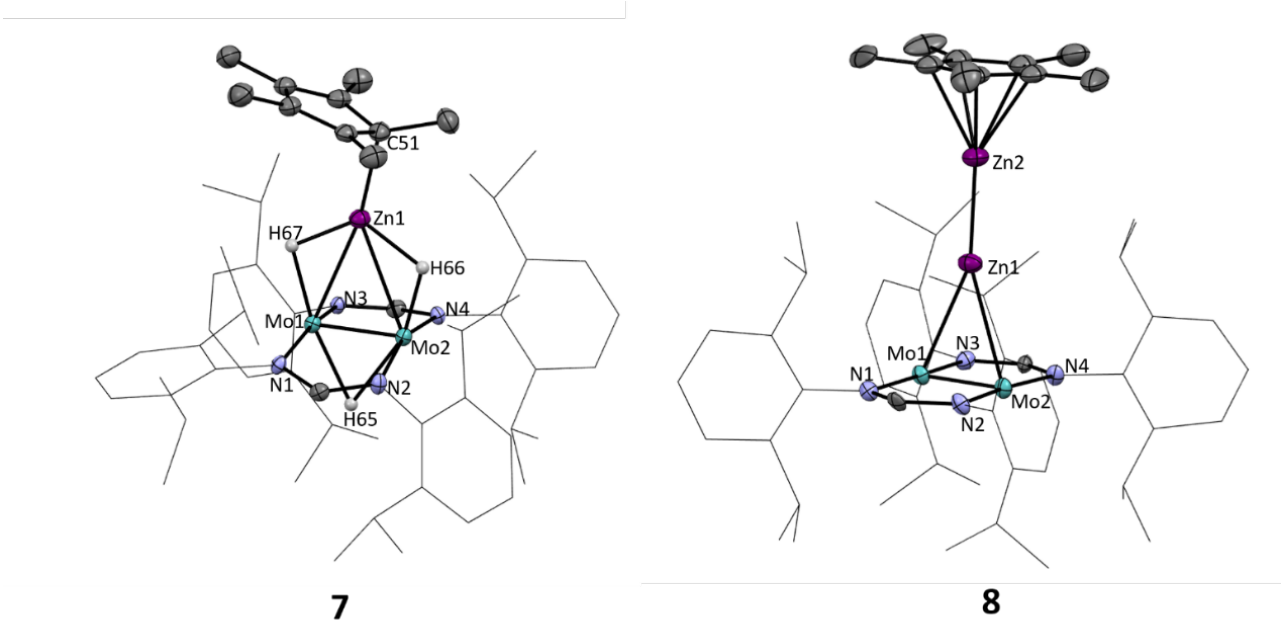

Figure 3. ORTEP representations of complexes **7** and **8**. Selected bond distances (Å) and angles (°): for complex **7**, 2.080(2) (Mo1–Mo2), 2.792(3) (Mo2–Zn1), 2.745(3) (Mo1–Zn1), 2.018(4) (Zn1–C51), 1.84(4) (Mo1–H67), 1.69(4) (Mo2–H66), 1.97(4) (Mo1–H65), 2.09(4) (Mo2–H65), 1.70(4) (Zn1–H67), 1.73(5) (Zn1–H66): for complex **8**, 2.075 (Mo1–Mo2), 2.850 (Mo1–Zn1), 2.828 (Mo2–Zn1), 2.347 (Zn1–Zn2).

Decamethyldizincocene, $Zn_2(\eta^5\text{-}C_5Me_5)_2$, behaved similarly and its reaction with **1** formed the yellow crystalline complex **8** (Scheme 3) which was isolated in yields around 35 %. The reaction was monitored by ^{1}H NMR experiments. After one hour heating at 60 °C, $Zn(C_5Me_5)_2$, C_5Me_5H and complex **7** were detected, accompanied by a finely divided grey precipitate of zinc metal. Following *ca*. 5 hours at 60 °C, the C_5Me_5H dehydrodimer, $C_{10}Me_{10}$, was also observed. It seems that this transformation involved the generation of C_5Me_5· radical, zinc-based radicals alike $(C_5Me_5)Zn$· and perhaps $(C_5Me_5)ZnZn$·.[28] An alternative procedure was obtained by performing the reaction at room temperature in the presence of H_2 (1 bar), conditions under which the yield for the formation of **8** increased to 60% (see experimental section). The $(\eta^5\text{-}C_5Me_5)ZnZn$ terminus of **8** is responsible for a ^{1}H signal at 2.31 pm and two $^{13}C\{^1H\}$ resonances with δ 11.1 ($C_5(\mathit{C}H_3)_5$) and 108.8 ppm (C_5Me_5). Unequivocal evidence for the proposed $Mo_2(\mu\text{-}H)_2Zn$ and $Mo(\mu\text{-}H)Mo$ bridging frameworks stems from the observation of the two ^{1}H NMR resonances at δ 4.72 and 6.42 ppm that appear as a broad triplet ($^2J_{HH}$ = 4.5 Hz) with relative intensity equivalent to 1H and as a doublet of 2H relative intensity, respectively. The solid-state molecular structure of the $Mo_2Zn_2H_3$ cluster was determined by X-ray diffraction studies (Figure 3) although the hydrides could not be located in the Fourier map due to crystal twinning. The Mo–Mo bond has a length of 2.075(2) Å, consistent, one more time, with a quadruple bond[33] and the distance between the Zn1 atom and the centroid of the Mo≣Mo bond of approximately 2.64 Å is comparable to the sum of covalent radii estimated for a Zn–Mo bond of 2.76 Å.[21] The direct Zn–Zn bond of the dizincocene reactant is preserved (2.347(4) Å, FSR = 0.96) and the Zn–η^5-C_5Me_5(centroid) separation is *ca*. 1.99 Å.

Structural and computational analysis of the Mo_2–H–E–R rings (E = Zn, Mg, Al, Li; R = H, Me, Et, Ph).

To analyze the bonding parameters of the Mo_2H triangle and the various Mo_2–R–E–H rings, with different main group electropositive metals E and where R can be a hydride or an alkyl or aryl group, it is convenient to use the interpenetration indices introduced by one of us recently.[36] In short, a penetration index for an A–B atom pair calibrates the degree of interpenetration of their van der Waals crusts, the portion of space comprised between a sphere with the van der Waals radius and the inner sphere with the covalent radius of an atom. Thus, a penetration index p_{AB} takes values of around 0% when the two atoms are at around the van der Waals distance (the sum of the van der Waals radii), reach values of around 100% when they are at bonding distance (the sum of their covalent radii), and appear at intermediate values for weak or non-covalent interactions. In the present analysis we include for comparison the data for the related Li compounds previously reported by us.[16b] The advantage of using penetration indices is that we can compare on an equal footing bonds between different atom pairs which, in the present case should allow us to obtain a general picture of the bonding within the Mo_2–R–E–H rings, with E = Li, Mg, Al, Zn, and R = H, Me, Et, Ph.

To complement the X-ray structural data we have optimized all the newly prepared compounds, including those that could not be submitted to an X-ray analysis, via DFT calculations (see Supporting Information for computational details). Given the good agreement between experimental and calculated interatomic distances, we use the latter for the present bonding analysis. This choice will allow us to have a larger number of data and reach more general conclusions, while avoiding the problems associated with the poor

localization of the hydrido bridges in the vicinity of heavy metal atoms. The bond distances and penetration indices for 14 compounds of this family are provided as Supporting Information (Table S1) and are summarized in Figure 4, where the ranges of values found are plotted for the five bonds of the ring, the E-L bond, and the distance between the center of the Mo–Mo bond and the metal E. The E–R bonds when R is a phenyl group are considered separately, since they correspond to a π coordination and have lower penetration than the purported σ-coordinated E–R groups (R = H, Me, Et).

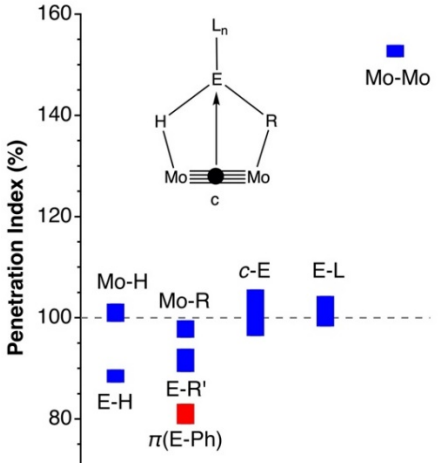

Figure 4. Ranges of penetration indices of the different bonds in the Mo_2REH rings (average ± one esd). R = H, Me, Et, Ph; R' = H, Me, Et.

The Mo–H–Mo triangle. In the compounds with a Mo–H–Mo bridge (**5** - **8**), there is a varying tendency of the hydride to be asymmetrically bonded to the Mo_2 unit (drawing **C**), with the short distance comprised between 1.795 and 2.025 Å, and the long one between 2.064 and 2.655 Å, showing a fair correlation (Figure 5) which suggests that a symmetric bridge should have two Mo-μH distances of about 2.1 Å, or penetration indices of about 91%, consistent with the values presented by the two other three-centre two-electron bonds, Mo–R–E and E–H–Mo.[37]

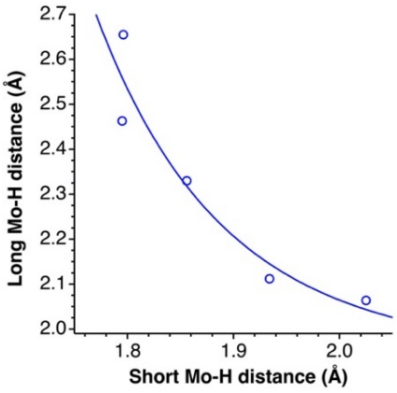

Figure 5. Correlation between the two Mo–H distances within the μH-Mo_2 triangle.

The E–L_n spectator bonds. The bonds between the electropositive metal E and the group(s) L attached to it, which do not participate directly in the bonding with the Mo_2 unit, are clearly unaffected by the formation of the adduct. This is shown by the penetration indices of around 100% in all compounds analyzed here, that comprise a wide variety of choices of E (Li, Mg, Al, Zn), R (H, Me, Et, Ph) and L (H, Me, Et, Ph, Cp*, ZnCp*, and thf).

Mo≣Mo bonds. The quadruple Mo≣Mo bonds present very large values of the penetration index, all within the pretty small range of 150 to 155%, to be compared to the large but clearly smaller values of triple Mo–Mo bonds found in the CSD of 131 (2) %. Such values point to the usefulness of the penetration index to discriminate different bond orders, and indicates that this parameter is a powerful way to calibrate a wide range of bonding situations, from weak van der Waals interactions all the way to pentuple metal-metal bonds.

The Mo–H–E bond sequence. Figure 4 shows that the Mo–H atom pairs have penetration indices in the range 96-103%, consistent with single bonds, whereas the interpenetration between the electropositive metal E and the same hydride is between 85 and 91%, indicative of weaker bonding interactions. This situation can be considered characteristic of a σ-Mo-H bond coordination to E (structure **A**), and is similar to that found in σ C–H bond coordination to transition metals M, as deduced from neutron diffraction bond distances, which yield C–H and M–H penetration indices in the ranges 96-100% and 59-84%, respectively, for M = Ru,[38] Mo[39] and W.[40]

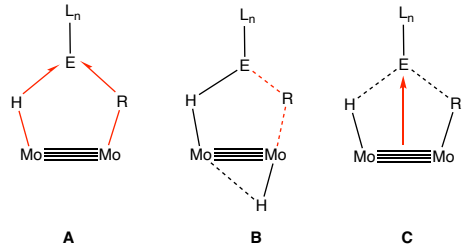

The Mo–R–E bond sequence. The Mo–R atom pairs (R = H, Me, Et) also present penetration indices of around 100% (96-102%) with only two exceptions, to be compared to the corresponding values for the E–R interaction, with interpenetrations in the range 83-95%. Thus, the results of the reactions can be interpreted as being in the way to alkyl transfer from E to Mo, retaining still a weaker E–R bonding interaction (structure **A**). Notably, the E–Ph interactions appear at still lower penetrations (79 - 83%), with the phenyl group coordinated to E in an η^1 or η^2 modes for E = Zn and Li, respectively.

The two exceptions regarding the Mo–R bonds correspond to compounds **6** and **7**, with smaller penetration indices (87 and 93%, respectively), a behaviour that must be attributed to the high asymmetry of the Mo_2H triangle and the consequently enhanced trans influence on the Mo–R bond, as schematically depicted in structure **B**.

Table 1. Major donor-acceptor interactions (kcal/mol)[a] disclosed by an NBO analysis for the Zn, Mg and Al adducts of Mo_2 presented in this work, together with the corresponding penetration indices (in %). Related values for the analogous Li compounds[16b] are given for comparison. The composition of each Mo_2REH ring is given by the symbols E/L/R.

Cpd.	**2**	**3**	**4**	**5**	**6**	**7**	**8**	**9**	**10**	**11**	**12**	**13**
E	Zn	Zn	Zn	Mg	Al	Zn	Zn	Li	Li	Li	Li	Li
L/R	Me/Me	Et/Et	H/Ph	Me/Me	Me_2/Me	Cp*/H	Zn/H	thf/Me	thf/Et	OEt_2/Ph	thf/Me	thf/Et
(Mo–Mo) → E												
p_{cE}	95	96	99	110	90	99	100	109	109	100	104	105
π(Mo–Mo) → σ*(E–L), σ*(E–H)	3.6	9.0	2.9	2.9	5.1	4.6	4.4	-	-	8.5	18.6	20.3
δ(Mo–Mo) → p_π(E) [b]	1.1	1.6	8.1	-	2.1	2.0	1.6	2.2	2.1	1.8	1.3	1.3
σ(Mo–Mo) → σ*(sp_yE–L), σ*(p_zE–H)	-	-	-	3.3	-	-	-	19.6	19.6	4.9	18.4	8.4
(Mo–R') → E												
p_{MoR}	96	100	102	97	87	93	99	100	100	100	99	98
σ(Mo–R) → σ*(E–L), σ*(p_zE–H)	65.3	25.7	7.8	27.6	-	-	34.3	29.0	25.5	18.2	43.7	34.1
p_{ER}	90	83	79	94	94	92	88	92	91	83	95	95
σ(E–R) → Mo	-	-	-	-	28.1	62.1		-	-	-	-	-
Ph → E												
p_{EC}			79							83		
σ(C-C) → σ*(E–H)	-	-	1.0	-	-	-	-	-	-	4.4	-	-
π(C-C) → σ*(E–H)	-	-	3.7	-	-	-	-	-	-	4.7	-	-
(Mo–H) → E or (E–H) → Mo												
p_{EH}	89	90	91	90	85	86	88	88	88	88	89	90
σ(Mo–H) → σ*(E–L) or σ*(E–R)	51.7	59.0		28.4	91.9	31.7*	34.3	44.8	41.8	50.1	55.3	50.4
σ(E–H) → σ*(Mo-H_b) or s(Mo)		-	89									

[a]) Only contributions equal or greater than 1.0 kcal/mol are included.

[b]) The δ(Mo–Mo) → p_π(E) donation can be to a non-bonding empty E atomic orbital (tricoordinated E), E-L antibonding (four-coordinated Al), or E-H antibonding orbital (ZnPh).

Through-ring Mo_2–E contact. If we consider the Mo–Mo bond to form roughly a cylinder of electron density with the same covalent and van der Waals radii than the Mo atoms, from the distance between the Mo–Mo centroid (*c*) and the electropositive metal E we can calculate a penetration index p_{cE}. This index is in all cases between 89 and 105% (Table 1 and Fig. 4), indicative of π-coordination of varying strength of the Mo≡Mo bond to E.

To obtain a molecular orbital description of the combination of apparent bonding situations exhibited by the Mo_2REH rings, we have carried out an NBO study of the donor-acceptor interactions. The computational details are provided as Supporting Information and the most significant results are presented in Table 1. All the interactions can be grouped in four families that can be discussed separately. A plot of the main donor-acceptor orbital interactions in the new compounds is provided as Supporting Information (Figure S1), since they are similar to those reported earlier for the lithium analogues,[16b] and only those orbitals responsible for the π-coordination of the phenyl rings to E in **4** and **11** are shown in Figure 6 to facilitate the discussion.

The delocalized E–R–Mo bond. The Mo–R penetration indices of around 100 % and the lower values found for the R–E pairs are reflected in the NBO results, which disclose a significant (Mo–R) → E donor-acceptor interaction (Table A), with associated interaction energies from 8 to 45 kcal/mol. In compounds **6** and **7**, in which the E–R penetration index is approximately equal or higher than the Mo-R one, the NBO analysis identifies the 3c-2e interaction as an (E–R) → Mo donation. In any event, it is clear that the Mo-R-E trio forms a 3c-2e bond.

The delocalized E–H–Mo bond. Similarly to what happens with the E–R–Mo system, the E–H–Mo trio is described by NBO as a (Mo–H) → E donation for all those compounds in which $p_{MoH} > p_{EH}$, and as an (E–H) → Mo donation for compound **4**, for which $p_{MoH} \lesssim p_{EH}$. These three atoms, therefore, form a second 3c-2e system in the ring.

The π coordination of the phenyl group to E. The side-on coordination of one of the phenyl groups in the Mo_2Zn compound **4** is reflected in the NBO results as a donor-acceptor interaction from a π(C–C) and, to a lesser extent, the σ(C–C) phenyl orbitals to E, via its σ*(E–H) orbital (Figure 6, above). A similar behaviour is found for the related LiPh adduct, the main structural difference being that in the Zn compound the phenyl group is closer to η^1 coordination, while in the Li one it coordinates in an η^2 mode. In the latter case, the acceptor orbital at E is σ*(E–L), where L is a terminal σ-bonded phenyl group (Figure 6, below).

The through-ring interaction between Mo_2 and E. Although the large penetration indices found between the centroid of the Mo–Mo bond and the electropositive metal E (Figure 4) might seem in principle to be due to the constraints of the cyclic system, the existence of direct bonding between Mo_2

and E is confirmed by the NBO identification of donor-acceptor interactions, mostly from the π and δ(Mo≣Mo) bonding orbitals for E = Zn and Al, while for the more electropositive Li and Mg atoms with slightly higher penetration indices, the dominant contribution comes from the σ(Mo≣Mo) orbital.

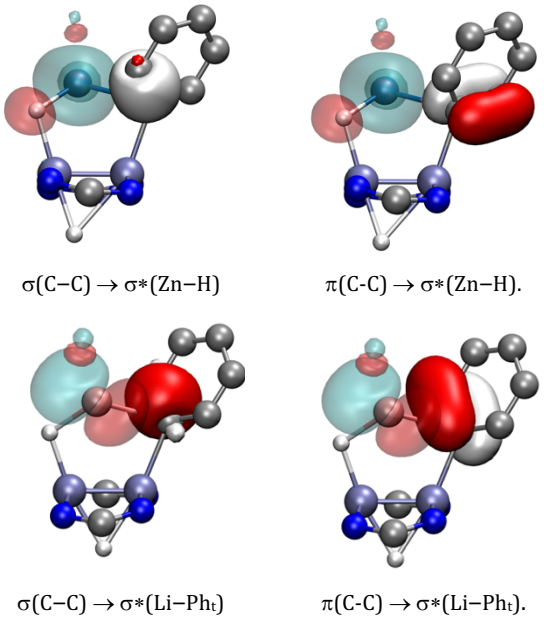

Figure 6. NBO depiction of the donor-acceptor interactions in compounds **4** (above) and **11** (below) from the σ (left) and π(C–C) bonding orbitals (right) of the phenyl group. The donor orbitals are represented by solid surfaces, and the acceptor ones by transparent lobes.

CONCLUSIONS

To conclude, we have analyzed the coordination of Zn–C bonds of $Zn(CH_3)_2$, $Zn(CH_2CH_3)_2$ and $Zn(C_6H_5)_2$ to the dimolybdenum core of complex **1**, as well as of the E–CH_3 bonds of $Mg(CH_3)_2$ and $Al(CH_3)_3$. All the new complexes obtained feature five-membered trimetallacyclic entities, $Mo_2E(C)(H)$, (E = Zn, Mg, Al), which exhibit similar electronic and bonding features to those derived from LiH and LiR. Zincocenes $Zn(C_5Me_5)_2$ and $Zn_2(\eta^5\text{-}C_5Me_5)_2$ behave differently to the previously mentioned zinc organyls. Our characterization studies reveal the presence of new molecular zinc hydrides, $(\eta^1(\pi)\text{-}C_5Me_5)Zn(H)$ and $(\eta^5\text{-}C_5Me_5)Zn–Zn(H)$, that, at present, do not appear to exist as free molecules. In our complexes, they become stabilized by coordination through the σ-Zn–H bond, supported intramolecularly by the adjacent Mo–H ⟶ Zn interaction, demonstrating the uniqueness of the *trans*-H–Mo≣Mo–H core. Our computational and structural analysis reveal that a general bonding pattern is found in the H–Mo≣Mo–E-R rings (E = Zn, Mg, Al, Li R =H, Me, Et, Ph), which includes 3 center-2 electron Mo-H-E and Mo-R-E bonds supplemented by π-coordination of the Mo≣Mo bond to the electropositive metal E.

EXPERIMENTAL SECTION

All manipulations were carried out using standard Schlenk (under Ar) and glovebox techniques (under high purity nitrogen). All solvents were dried and degassed prior to use. Toluene (C_7H_8) and *n*-pentane (C_5H_{12}) were distilled under nitrogen over sodium. Tetrahydrofuran (thf) was distilled under nitrogen over sodium/benzophenone. Benzene-d_6 and toluene-d_8 were dried over 4 Å molecular sieves. Thf-d_8 was distilled over sodium under argon atmosphere and stored under 4 Å molecular sieves. Solution NMR spectra were recorded on Bruker DRX-400 and DRX-500 spectrometers. Spectra were referenced to external $SiMe_4$ (δ: 0 ppm) using the residual proton solvent peaks as internal standards (^{1}H NMR experiments), or the characteristic resonances of the solvent nuclei (^{13}C NMR experiments). Spectral assignments were made by routine one- and two-dimensional NMR experiments, where appropriate. For elemental analyses a LECO TruSpec CHN elementary analyzer was utilized. Complex **1** was prepared according to the literature.[22]

$[Mo_2(\mu\text{-}HZnMe_2)_2(\mu\text{-}Ad^{Dipp2})_2]$ (**2**): Complex $[Mo_2(H)_2(\mu\text{-}Ad^{Dipp2})_2(thf)_2]$ (**1**) (30 mg, 0.03 mmol) was dissolved in toluene (3 mL) at room temperature. A 0.3 mL solution of $ZnMe_2$ in toluene (0.2 M) was added slowly at room temperature. The solution changed color immediately to yellow. The solvent was then removed under vacuum. The residue was washed with pentane and the yellow solid obtained was dried under vacuum (15 mg, 45 % yield). ^{1}H NMR (500 MHz, C_6D_6, 25 °C) δ (ppm): -0.46 (s, 3 H, Mo(μ-Me)Zn), 0.32 (s, 3 H, ZnMe), 1.05, 1.10, 1.31, 1.39 (d, 48 H, 12 H each, $^3J_{HH}$ = 6.7 Hz, CH*Me*$_2$), 2.83, 3.87 (sept, 8 H, 4 H each, $^3J_{HH}$ = 6.7 Hz, C*H*Me$_2$), 5.54 (s, 2 H, Mo(μ-H)Zn), 6.98-7.11 (m, 12 H, *m*, *p*-Dipp), 8.12 (s, 2 H, NC(H)N).^{13}C{^{1}H} NMR (100 MHz, C_6D_6, 25 °C) δ (ppm): -5.4 (ZnMe, $^1J_{CH}$ = 123 Hz), 3.0 (Mo(μ-Me)Zn, $^1J_{CH}$ = 126 Hz), 24.5, 24.6, 25.4, 28.8 (CH*Me*$_2$), 29.2, 29.3 (*C*HMe$_2$), 123.9, 124.8, 126.6 (*m*-Dipp, *p*-Dipp), 143.4, 144.0, 145.1 (*o*-Dipp, *ipso*-Dipp), 163.8 (NC(H)N). Elemental Analysis (%) for $C_{54}H_{84}Mo_2N_4Zn_2$: Calc. C, 58.3; H, 7.6; N, 5.0. Exp. C, 58.5; H, 7.2; N, 5.0.

$[Mo_2(\mu\text{-}HZnEt_2)_2(\mu\text{-}Ad^{Dipp2})_2]$ (**3**): Complex $[Mo_2(H)_2(\mu\text{-}Ad^{Dipp2})_2(thf)_2]$ (**1**) (30 mg, 0.03 mmol) was dissolved in toluene (3 mL) at room temperature. 0.6 mL of a solution of $ZnEt_2$ in hexane (0.1 M) was added slowly at room temperature. The solution color changed immediately to yellow. By slow evaporation of the solvent, yellow crystals were obtained, washed with cold pentane and isolated in 55% yield (19 mg). ^{1}H NMR (400 MHz, C_6D_6, 25 °C) δ (ppm): -1.77 (t, 6 H, $^3J_{HH}$ = 7.7 Hz, CH_3, Mo(μ-CH_2*C*H_3)Zn), 1.10-1.19 (m, 8 H, CH_2, Mo(*C*$H_2$$CH_3$)Zn, Zn*C*$H_2$$CH_3$, detected by COSY experiments), 1.08, 1.23, 1.31, 1.48 (d, 48 H, 12 H each, $^3J_{HH}$ = 6.9 Hz, CH*Me*$_2$), 1.95 (t, 6 H, CH_3, $^3J_{HH}$ = 7.9 Hz, Zn*C*$H_2$$CH_3$), 3.04, 4.11 (sept, 8 H, 4 H each, $^3J_{HH}$ = 6.9 Hz, C*H*Me$_2$), 5.46 (s, 2 H, Mo(μ-H)Zn), 6.94-7.25 (m, 12 H, *m*, *p*-Dipp), 8.18 (s, 2 H, NC(H)N). ^{13}C{^{1}H} NMR (100 MHz, C_6D_6, 25 °C) δ (ppm): -6.8 (br, CH_3, Mo(μ-CH_2*C*H_3)Zn), 2.9, 8.5 (CH_2, Zn*C*$H_2$$CH_3$, Mo(μ-*C*$H_2$$CH_3$)Zn), 13.4 ($CH_3$, Zn$CH_2$*C*$H_3$), 24.5, 24.6, 25.9, 29.1 (CH*Me*$_2$), 29.2, 29.3 (*C*HMe$_2$), 123.9, 124.4, 126.6 (*m*-Dipp, *p*-Dipp), 143.6, 144.3, 145.8 (*o*-Dipp, *ipso*-Dipp), 163.4 (NC(H)N). Elemental Analysis (%) for $C_{58}H_{92}Mo_2N_4Zn_2$: Calc. C, 59.6; H, 7.9; N, 4.8. Exp. C, 59.7; H, 7.8; N, 4.9.

$[Mo_2(\mu\text{-}HZnPh_2)(\mu\text{-}H)(\mu\text{-}Ad^{Dipp2})_2]$ (**4**): Complex $[Mo_2(H)_2(\mu\text{-}Ad^{Dipp2})_2(thf)_2]$ (**1**) (30 mg, 0.03 mmol) and $ZnPh_2$ (7 mg, 0.03 mmol)[34] were dissolved in toluene (3 mL) at room temperature. The solution changed colour immediately to brown-yellow. The solvent was then removed under vacuum. The residue was washed with pentane and the orangish brown solid obtained was dried under vacuum and isolated in 40 % yield (14 mg). Suitable crystals for x-ray diffraction studies were obtained from a diethylether solution placed inside the glovebox freezer at -30 °C for 2 days. ^{1}H NMR (400 MHz, C_6D_6, 25 °C) δ (ppm): 0.42, 0.50 (m, 6 H each, CH*Me*$_2$), 0.62 (d, 6 H, $^3J_{HH}$ = 6.9 Hz, CH*Me*$_2$), 1.12-1.33 (m, 30 H, CH*Me*$_2$), 3.06, 3.74 (sept, 2 H each, $^3J_{HH}$ = 6.9 Hz, C*H*Me$_2$), 3.84 (m, 3 H, C*H*Me$_2$ + Mo(μ-H)Mo), 4.32 (sept, 2 H, $^3J_{HH}$ = 6.9 Hz, C*H*Me$_2$), 6.98-7.24 (m, 18 H, *m*, *p*-Dipp + $ZnPh_2$), 7.35 (d, 1 H, $^2J_{HH}$ = 4 Hz, Mo(μ-H)Zn), 7.58 (br, 2 H, $ZnPh_2$), 7.82 (br, 1 H, $ZnPh_2$), 8.60 (s, 2 H, NC(H)N). ^{1}H NMR (400 MHz, C_6D_6, 45 °C) δ (ppm): 3.87 (d, 1 H, $^2J_{HH}$ = 4 Hz, Mo(μ-H)Mo), 7.32 (d, 1 H, $^2J_{HH}$ = 4 Hz, Mo(μ-H)Zn). ^{13}C{^{1}H} NMR (100 MHz, C_6D_6, 25 °C) δ (ppm): 23.2, 24.8, 24.9, 25.1, 25.3,

25.4, 25.6, 26.5 (CH*Me*$_2$), 28.5, 28.7, 28.8, 30.2 (*C*HMe$_2$), 124.0, 124.4, 124.5, 124.6, 126.8, 126.9, 127.1, 127.2, 127.6, 129.9, 130.9, 138.1 (*m*-Dipp, *p*-Dipp, *m*-ZnPh$_2$, *p*-ZnPh$_2$, *o*-ZnPh$_2$), 143.2, 143.6, 143.8, 143.9, 144.5, 144.6 (*o*-Dipp, *ipso*-Dipp), 155.0, 160.1 (*ipso*-ZnPh$_2$), 165.2 (NC(H)N). Elemental Analysis (%) for $C_{62}H_{82}Mo_2N_4Zn$: Calc. C, 65.3; H, 7.3; N, 4.9. Exp. C, 65.0; H, 7.6; N, 4.6.

[Mo$_2$(μ-HMgMe$_2$)(μ-H)(μ-Ad^{Dipp2})$_2$] (**5**): MgMe$_2$·Et$_2$O[34] (4 mg, 0.03 mmol) and complex [Mo$_2$(H)$_2$(μ-Ad^{Dipp2})$_2$(thf)$_2$] (**1**) (30 mg, 0.03 mmol), were dissolved in a mixture of toluene and diethyl ether (3:3 mL). The red solution was stirred for 30 minutes at room temperature. Then, the solvent was removed under vacuum and the orange residue was washed with cold pentane to afford a brown solid (8 mg, 27 % yield). The product is unstable in solution at room temperature, so that complete decomposition occurred after 3 hours in C_6D_6, forming methane (0.16 ppm singlet in C_6D_6) and an undetermined mixture of products. ^{1}H NMR (400 MHz, tol-d_8, -20 °C) δ (ppm): -0.29 (br s, 3 H, Mo(μ-Me)Mg), -0.01 (br s, 3 H, MgMe), 0.39, 0.49, 1.15 (d, 6 H each, $^3J_{HH}$= 6.3 Hz, CH*Me*$_2$), 1.21 (m, 12 H, CH*Me*$_2$), 1.28 (d, 6 H, $^3J_{HH}$= 6.3 Hz, CH*Me*$_2$), 1.50 (m, 12 H, CH*Me*$_2$), 3.12 (d, 1 H, $^2J_{HH}$= 6.6 Hz, Mo(μ-H)Mo), 3.48, 3.63, 3.89, 4.21 (sept, 2 H each, $^3J_{HH}$ = 6.3 Hz, C*H*Me$_2$), 5.24 (d, 1 H, $^2J_{HH}$= 6.6 Hz, Mo(μ-H)Mg), 6.90-7.04 (m, 12 H, *m*, *p*-Dipp), 8.64 (s, 2 H, NC(H)N). ^{13}C{^{1}H} NMR (100 MHz, tol-d_8, -20 °C) δ (ppm): -9.4 (MgMe), $^1J_{CH}$ = 110 Hz), 2.8 (Mg(μ-Me)Mo, $^1J_{CH}$ = 114 Hz), 22.9, 24.0, 24.4, 24.8, 25.1, 25.7, 25.9, 26.6 (CH*Me*$_2$), 26.9, 28.3, 28.4, 28.6 (*C*HMe$_2$), 124.0, 124.1, 124.3, 124.5, 126.2, 126.4 (*m*-Dipp, *p*-Dipp), 143.2, 143.3, 143.6, 143.8, 144.1, 144.4 (*ipso*-Dipp, *o*-Dipp), 164.1 (NC(H)N). Elemental Analysis (%) for $C_{52}H_{78}MgMo_2N_4$: Calc. C, 64.0; H, 8.1; N, 5.7. Exp. C, 64.1; H, 8.2; N, 5.5.

[Mo$_2$(μ-H)(μ-AlMe$_3$H)(μ-Ad^{Dipp2})$_2$] (**6**): Complex [Mo$_2$(H)$_2$(μ-Ad^{Dipp2})$_2$(thf)$_2$] (**1**) (50 mg, 0.05 mmol) was dissolved in toluene (5 mL) and 0.08 mL of AlMe$_3$ (1 M solution in toluene) was added at room temperature. After five minutes of stirring at room temperature, the solution changed from red to dark orange. The solvent was removed under vacuum to afford a dark microcrystalline orange solid which was washed with cold pentane (2x1 mL) to obtain an orange solid in 58 % yield (29 mg). Crystals suitable for x-ray diffraction studies were obtained by slow evaporation of a mixture of benzene and pentane (1:2) inside the glovebox under N_2 atmosphere. ^{1}H NMR (400 MHz, C_6D_6, 25 °C) δ (ppm): -0.11 (s, 3 H, Mo(μ-Me)Al), 0.14 (s, 6 H, AlMe$_2$), 0.54, 0.58, 0.99 (d, 6 H each, $^3J_{HH}$ = 6.7 Hz, CH*Me*$_2$), 1.21 (m, 18 H, CH*Me*$_2$), 1.36, 1.40 (d, 6 H each, $^3J_{HH}$ = 6.7 Hz, CH*Me*$_2$), 3.04 (d, 1 H, Mo(μ-H)Mo, $^2J_{HH}$ = 10.0 Hz), 3.34, 3.52, 3.92, 4.35 (sept, 2 H each, $^3J_{HH}$ = 6.7 Hz, C*H*Me$_2$), 5.64 (d, 1 H, Mo(μ-H)Al, $^2J_{HH}$ = 10.0 Hz), 6.94-7.08 (m, 12 H, *m*, *p*-Dipp), 8.71 (s, 2 H, NC(H)N).^{13}C{^{1}H} NMR (100 MHz, C_6D_6, 25 °C) δ (ppm): -2.6 (AlMe$_2$, $^1J_{CH}$ = 112 Hz), 11.3 (Al(μ-Me)Mo, $^1J_{CH}$ = 116 Hz), 23.8, 24.0, 24.7, 25.0, 25.7, 26.0, 26.2, 27.1 (CH*Me*$_2$), 28.0, 28.3, 28.7, 29.1 (*C*HMe$_2$), 123.9, 124.1, 124.8, 125.0, 126.8, 126.9 (*m*-Dipp, *p*-Dipp), 143.3, 143.5, 143.7, 143.8, 144.3, 144.3 (*ipso*-Dipp, *o*-Dipp), 165.3 (NC(H)N). Elemental Analysis (%) for $C_{53}H_{81}AlMo_2N_4$: Calc. C, 64.1; H, 8.2; N, 5.6. Exp. C, 64.1; H, 8.3; N, 5.2.

[Mo$_2$(μ-H$_2$ZnCp*)(μ-H)(μ-Ad^{Dipp2})$_2$] (**7**): Method A: Complex [Mo$_2$(H)$_2$(μ-Ad^{Dipp2})$_2$(thf)$_2$] (**1**) (30 mg, 0.03 mmol) and ZnCp*$_2$[35] (10 mg, 0.03 mmol) were dissolved in toluene (3 mL) at room temperature inside the glovebox and transferred to an ampoule. After stirring for 8 hours at 60 °C, toluene was removed under vacuum and diethylether was added. The brown solution formed was filtered and pentane (1 mL) was added. Orange crystals were obtained by slow evaporation of the mixture and washed with cold pentane (15 mg, 44 % yield). Suitable crystals for X-ray diffraction were obtained from a diethylether solution placed inside the glovebox freezer at -30 °C for 2 days. Method B: Complex [Mo$_2$(H)$_2$(μ-Ad^{Dipp2})$_2$(thf)$_2$] (**1**) (50 mg, 0.05 mmol) and Zn(C$_5$Me$_5$)$_2$ (17 mg, 0.05 mmol) were dissolved in toluene (5 mL) at room temperature inside the glovebox and transferred to an ampoule. The N_2 atmosphere was substituted by H_2 (1 bar) and the solution was stirred for 3 hours at room temperature. Then, the toluene was removed under vacuum and the residue was extracted with diethyl ether (5 mL). Pentane (2 mL) was added to the orange ether solution and placed overnight in the freezer to precipitate yellow orangish microcrystals which were washed with cold pentane and isolated in 60 % yield (33 mg). ^{1}H NMR (400 MHz, C_6D_6, 25 °C) δ (ppm): 0.43, 1.14, 1.17, 1.37 (d, 48 H, 12 H each, $^3J_{HH}$ = 6.7 Hz, CH*Me*$_2$), 2.33 (s, 15 H, CH$_3$, C$_5$Me$_5$), 3.28 (br t, 1 H, Mo(μ-H)Mo), 3.38, 3.84 (sept, 8 H, 4 H each, $^3J_{HH}$ = 6.7 Hz, C*H*Me$_2$), 5.19 (d, 2 H, $^2J_{HH}$ = 4 Hz, Mo(μ-H)Zn), 6.91-7.06 (m, 12 H, *m*, *p*-Dipp), 8.53 (s, 2 H, NC(H)N). ^{13}C{^{1}H} NMR (100 MHz, C_6D_6, 25 °C) δ (ppm): 12.8 (C$_5$*Me$_5$*), 24.3, 25.4, 25.5, 26.3 (CH*Me*$_2$), 28.6, 28.9 (*C*HMe$_2$), 115.5 (*C*$_5$Me$_5$), 124.0, 124.8, 126.8 (*m*-Dipp, *p*-Dipp), 143.3, 143.8, 143.8 (*o*-Dipp, *ipso*-Dipp), 165.7 (NC(H)N). Elemental Analysis (%) for $C_{60}H_{88}Mo_2N_4Zn$: Calc. C, 64.2; H, 7.9; N, 5.0. Exp. C, 63.7; H, 8.3; N, 4.2.

[Mo$_2$(μ-H$_2$Zn$_2$Cp*)(μ-H)(μ-Ad^{Dipp2})$_2$] (**8**): Method A: Complex [Mo$_2$(H)$_2$(μ-Ad^{Dipp2})$_2$(thf)$_2$] (**1**) (30 mg, 0.03 mmol) and Zn$_2$Cp*$_2$ (12 mg, 0.03 mmol) were dissolved in toluene (3 mL) at room temperature inside the glovebox and transferred to an ampoule. After stirring for 8 hours at 60 °C, toluene was removed under vacuum and diethyl ether (2 mL) was added. The yellow solution formed was filtered and concentrated to the half. Yellow crystals were obtained after 1 day at the freezer inside the glovebox at -30 ºC. The crystals were washed with cold pentane and isolated in 35% yield (13 mg). Method B: Complex [Mo$_2$(H)$_2$(μ-Ad^{Dipp2})$_2$(thf)$_2$] (**1**) (50 mg, 0.05 mmol) and Zn$_2$(η^5-C$_5$Me$_5$)$_2$ (20 mg, 0.05 mmol) were dissolved in toluene (5 mL) at room temperature inside the glovebox and transferred to an ampoule. The N_2 atmosphere was substituted by H_2 (1 bar) and the solution was stirred for 4 hours at room temperature. Then, the toluene was removed under vacuum and the residue was extracted with diethyl ether (5 mL). Pentane (2 mL) was added to the ether orange solution and placed overnight in the freezer to precipitate yellow microcrystals which were washed with cold pentane and isolated in 55 % yield (32 mg). ^{1}H NMR (400 MHz, C_6D_6, 25 °C) δ (ppm): 0.79, 1.30, 1.37, 1.41 (d, 48 H, 12 H each, $^3J_{HH}$ = 6.8 Hz, CH*Me*$_2$), 2.31 (s, 15 H, CH$_3$, C$_5$Me$_5$), 3.66, 4.19 (sept, 8 H, 4 H each, $^3J_{HH}$ = 6.8 Hz, C*H*Me$_2$), 4.72 (br t, 1 H, $^2J_{HH}$ = 4.5 Hz, Mo(μ-H)Mo), 6.42 (d, 2 H, $^2J_{HH}$ = 4.5 Hz, Mo(μ-H)Zn), 7.00, 7.13 (m, 8 H and 4 H each, *m*, *p*-Dipp), 8.30 (s, 2 H, NC(H)N). ^{13}C{^{1}H} NMR (100 MHz, C_6D_6, 25 °C) δ (ppm): 11.1 (C$_5$*Me$_5$*), 25.0, 25.2, 25.7, 26.0 (CH*Me*$_2$), 28.5, 28.7 (*C*HMe$_2$), 108.8 (*C*$_5$Me$_5$), 123.5, 124.2, 127.1 (*m*-Dipp, *p*-Dipp), 143.5, 144.9, 145.0 (*o*-Dipp, *ipso*-Dipp), 162.6 (NC(H)N). Elemental Analysis (%) for $C_{60}H_{88}Mo_2N_4Zn_2$: Calc. C, 60.7; H, 7.5; N, 4.7. Exp. C, 60.7; H, 7.6; N, 4.1.

ASSOCIATED CONTENT

Supporting Information

Supporting information includes NMR spectra of the new compounds, X-ray crystallography details, computational details and atomic coordinates for the optimized geometries of the compounds.

AUTHOR INFORMATION

Corresponding Author

* (Word Style "FA_Corresponding_Author_Footnote"). Give contact information for the author(s) to whom correspondence should be addressed.

Notes

Any additional relevant notes should be placed here.

ACKNOWLEDGMENT

This work has been supported by the Spanish Ministry of Economy and Competitiveness (PID2019-110856GA-I00 and PGC2018-093863-B-C21), the Spanish Structures of Excellence María de Maeztu program (grant MDM-2017-0767) and the Generalitat de Catalunya–AGAUR (grant 2017-SGR-1289). M. P.-J. thanks the Spanish Ministry of Education, the Ministry of Universities and Ministry of Science and Innovation for an FPU PhD fellowship.

REFERENCES

(1) (a) Riddlestone, I. M.; Abdalla, J. A.; Aldridge, S. Coordination and Activation of E-H Bonds (E= B, Al, Ga) at Transition Metal Centers. *Adv. Organomet. Chem.* **2015**, *63*, 1-38. (b) Butler, M. J.; Crimmin, M.R. Magnesium, zinc, aluminium and gallium hydride complexes of the transition metals. *Chem. Commun.* **2017**, *53*, 1348-1365. (c) Roy, M. M. D. Omaña, A. A.; Wilson, A. S. S.; Hill, M. S. Aldridge, S.; Rivard, E. Molecular Main Group Metal Hydrides. *Chem. Rev.* **2021**, DOI: 10.1021/acs.chemrev.1c00278.

(2) Batuecas, M.; Nikolaus, G.; Crimmin, M. R. Catalytic C–H to C–M (M= Al, Mg) bond transformations with heterometallic complexes. *Chem. Sci.* **2021**, *12*, 1993-2000.

(3) Fischer, K.; Jonas, K.; Misbach, P.; Stabba, R.; Wilke, G. The "nickel effect". *Angew. Chem. Int. Ed. Eng.* **1973**, *12*, 943-953.

(4) (a) Haas, D.; Hammann, J. M.; Greiner, R.; Knochel, P. Recent Developments in Negishi Cross-Coupling Reactions. *ACS Catalysis* **2016**, 6, 1540-1552. (b) Knappke, C. E.; von Wangelin, A. J. 35 years of palladium-catalyzed cross-coupling with Grignard reagents: how far have we come? *Chem. Soc. Rev*. **2011**, *40*, 4948-4962. (c) Minami, H.; Saito, T.; Wang, C.; Uchiyama, M. Organoaluminum-Mediated Direct Cross-Coupling Reactions. *Angew. Chem. Int. Ed*. **2015**, *54*, 4665-4668.

(5) (a) García-Melchor, M.; Fuentes, B.; Lledós, A.; Casares, J. A.; Ujaque, G.; Espinet, P. Cationic Intermediates in the Pd-Catalyzed Negishi Coupling. Kinetic and Density Functional Theory Study of Alternative Transmetalation Pathways in the Me–Me Coupling of $ZnMe_2$ and trans-$[PdMeCl(PMePh_2)_2]$. *J. Am. Chem. Soc.***2011**, *133*, 13519-13526. (b) Paenurk, E.; Gershoni-Poranne, R.; Chen, P. Trends in Metallophilic Bonding in Pd–Zn and Pd–Cu Complexes. *Organometallics* **2017**, *36*, 4854–4863.

(6) (a) Kaschube, W.; Pörschke, K. -R.; Angermund, Krüger, C.; Wilke, G. Zur Lewis-Acidität von Nickel (0), X. Diorganylmagnesium-Komplexe von Nickel(0):$(TMEDA)MgCH_3(\mu\text{-}CH_3)Ni(C_2H_4)_2$ *Chem. Ber.* **1988**, *121*, 1921-1929. (b) Jonas, K.; Koepe, G.; Krüger, C. Heterometallic dinuclear complexes by ethene displacement with Grignard compounds or diorganomagnesium compounds. *Angew. Chem. Int. Ed. Engl.* **1986**, *25*, 923-925.

(7) Chan, M. C. W.; Gibson, V. C.; Cole, J. M.; Howard, J. A. K. Novel μ-methyl complexes of vanadium and their relevance to bimolecular deactivation of homogeneous imidovanadium polymerisation catalysts. *Chem. Commun.* **1997**, 2345-2346.

(8) Khan, S. I.; Edwards, P. G.; Yuan, H. S. H.; Bau, R. Structures of the copper-containing Cu_4MgPh_6 and $[Cu_4LiPh_6]$-clusters: first example of a magnesium-containing transition-metal cluster compound. *J. Am. Chem. Soc.* **1985**, *107*, 1682-1684.

(9) Bolton, P. D.; Clot, E.; Cowley, A. R.; Mountford, P. $AlMe_3$ and $ZnMe_2$ adducts of a titanium imido methyl cation: A combined crystallographic, spectroscopic, and DFT study. *J. Am. Chem. Soc*. **2006**, *128*, 15005-15018.

(10) (a) Ogoshi, S.; Ueta, M.; Arai, T.; Kurosawa, H. $AlMe_3$-promoted oxidative cyclization of η^2-alkene and η^2-ketone on Nickel (0). Observation of intermediate in methyl transfer process. *J. Am. Chem. Soc*. **2005**, *127*, 12810-12811. (b) Weng, Z.; Teo, S.; Koh, L. L.; Hor, T. S. A. A structurally characterized Ni–Al methyl-bridged complex with catalytic ethylene oligomerization activity. *Chem. Commun.* **2006**, 1319-1321.

(11) (a) Mulvey, R.; Mongin, F.; Uchiyama, M.; Kondo, Y. Deprotonative metalation using ate compounds: synergy, synthesis, and structure building. *Angew. Chem. Int. Ed.* **2007**, *46*, 3802-3824. (b) Armstrong, D. R.; Dougan, C.; Graham, D. V.; Hevia, E.; Kennedy, A. R. Synthesis and Structural Elucidation of Alkyl, Amido, and Mixed Alkyl–Amido "Highly-Coordinated" Zincates. *Organometallics* **2008**, *27*, 6063-6070. (c) Merkel, S.; Stern, D.; Henn, J.; Stalke, D. Solvent-Separated and Contact Ion Pairs of Parent Lithium Trimethyl Zincate. *Angew. Chem. Int. Ed.* **2009**, *48*, 6350-6353. (d) Barley, H. R. L.; Clegg, W.; Dale, S. H.; Hevia, E.; Honeyman, G. W.; Kennedy, A. R.; Mulvey, R. E. Alkali-Metal-Mediated Zincation of Ferrocene: Synthesis, Structure, and Reactivity of a Lithium Tmp/Zincate Reagent. *Angew. Chem. Int. Ed*. **2005**, *44*, 6018-6021.

(12) Hratchian, H. P.; Chowdhury, S. K.; Gutiérrez-García, V. M.; Amarasinghe, K. K. D.; Heeg, M. J.; Bernhard Schlegel, H.; Montgomery, J. Combined experimental and computational investigation of the mechanism of nickel-catalyzed three-component addition processes. *Organometallics* **2004**, *23*, 4636-4646.

(13) Negishi, E. -i. Magical power of transition metals: past, present, and future (Nobel Lecture). *Angew. Chem. Int. Ed*. **2011**, *50*, 6738-6764.

(14) (a) Oeschger, R. J.; Chen, P. A Heterobimetallic Pd–Zn Complex: Study of a d8–d10 Bond in Solid State, in Solution, and in Silico. *Organometallics* **2017**, *36*, 1465–1468. (b) Liberman-Martin, A. L.; Levine, D. S.; Ziegler, M. S.; Bergman, R. G.; Tilley, T. D. Lewis Acid–Base Interactions Between Platinum(II) Diaryl Complexes and Bis(perfluorophenyl)zinc: Strongly Accelerated Reductive Elimination Induced by a Z-type Ligand. *Chem. Commun*. **2016**, *52*, 7039-7042.

(15) (a) Pozo, J.; Salas, G.; Álvarez, R.; Casares, J. A.; Espinet, P. The Negishi catalysis: full study of the complications in the transmetalation step and consequences for the coupling products. *Organometallics* **2016**, *35*, 3604-3611; b) Pozo, J.; Gioria, E.; Casares, J. A.; Álvarez, R.; Espinet, P. Organometallic Nucleophiles and Pd: What Makes $ZnMe_2$ Different? Is Au Like Zn? *Organometallics* **2015**, *34*, 3120-3128. (c) Casares, J. A.; Espinet, P.; Fuentes, B.; Salas, G. *J. Am. Chem. Soc.* **2007**, *129*, 3508-3509; (d) Fuentes, B.; García-Melchor, M.; Lledós, A.; Maseras, F.; Casares, J.; Ujaque, G.; Espinet, P. Palladium round trip in the Negishi coupling of trans-$[PdMeCl(PMePh_2)_2]$ with ZnMeCl: an experimental and DFT study of the transmetalation step. *Chem. Eur. J.* **2010**, *16*, 8596-8599.

(16) (a) Pérez-Jiménez, M.; Curado, N.; Maya, C.; Campos, J.; Jover, J.; Álvarez, S.; Carmona, E. Coordination of LiH Molecules to Mo≣Mo Bonds: Experimental and Computational Studies on Mo_2LiH_2, $Mo_2Li_2H_4$, and $Mo_6Li_9H_{18}$ Clusters *J. Am. Chem. Soc.* **2021**, *143*, 5222-5230. (b) Pérez-Jiménez, M.; Campos, J.; Jover, J.; Alvarez, S.; Carmona, E., Supported σ-Complexes of Li—C Bonds from Coordination of Monomeric Molecules of $LiCH_3$, $LiCH_2CH_3$ and LiC_6H_5 to Mo-Mo Bonds. *Angew. Chem. Int. Ed.* **2022**, *61,* e2021160.

(17) Campos, J. Bimetallic cooperation across the periodic table. *Nat. Rev. Chem.* **2020**, *4*, 696-702.

(18) (a) Kosai, T.; Iwamoto, T. Stable Push–Pull Disilene: Substantial Donor–Acceptor Interactions through the Si═Si Double Bond. *J. Am. Chem. Soc.* **2017**, *139*, 18146-18149. (b) Swarnakar, A. K.; Ferguson, M. J.; McDonald, R.; Rivard, E. Transition metal-mediated donor–acceptor coordination of low-oxidation state Group 14 element halides. *Dalton Trans.* **2016**, *45*, 6071-6078. (c) Al-Rafia, S. I.; Malcolm, A. C.; Liew, S. K.; Ferguson, M. J.; Rivard, E. Stabilization of the heavy methylene analogues, GeH_2 and SnH_2, within the coordination sphere of a transition metal. *J. Am. Chem. Soc.* **2011**, *133*, 777-779.

(19) Green, J. C.; Green, M. L. H.; Parkin, G. The occurrence and representation of three-centre two-electron bonds in covalent inorganic compounds. *Chem. Commun*. **2012**, *48*, 11481-11503.

(20) Hernán-Gómez, A.; Orr, S. A.; Uzelac, M.; Kennedy, A. R.; Barroso, S.; Jusseau, X.; Lemaire, S.; Farina, V.; Hevia, E. Exploiting synergistic effects in organozinc chemistry for direct stereoselective

C-glycosylation reactions at room temperature. *Angew. Chem. Int. Ed.* **2018**, *57*, 10630-10634.
(21) Cordero, B.; Gómez, V.; Platero-Prats, A. E.; Revés, M.; Echeverría, J.; Cremades, E.; Barragan, F.; Álvarez, S. Covalent radii revisited. *Dalton Trans*. **2008**, 2832-2838.
(22) Pérez-Jiménez, M.; Curado, N.; Maya, C.; Campos, J.; Ruiz, E.; Álvarez, S.; Carmona, E. Experimental and Computational Studies on Quadruply Bonded Dimolybdenum Complexes with Terminal and Bridging Hydride Ligands. *Chem. Eur. J.* **2021**, *27*, 6569-6578.
(23) (a) Yousef, R. I.; Walfort, B.; Rüffer, T.; Wagner, C.; Schmidt, H.; Herzog, R.; Steinborn, D. Synthesis, characterization and Schlenk equilibrium studies of methylmagnesium compounds with O-and N-donor ligands–the unexpected behavior of [MgMeBr(pmdta)](pmdta=N,N,N′,N″,N″-pentamethyldiethylenetriamine). *J. Organomet. Chem*. **2005**, *690*, 1178-1191. (b) Schlenk, W.; Schlenk, W. Über die Konstitution der Grignardschen Magnesiumverbindungen. *Chem. Ber*. **1929**, *62*, 920-924.
(24) Resa, I.; Carmona, E.; Gutierrez-Puebla, E.; Monge, A. Decamethyldizincocene, a stable compound of Zn (I) with a Zn-Zn bond. *Science* **2004**, *305*, 1136-1138.
(25) Freitag, K.; Banh, H.; Ganesamoorthy, C.; Gemel, C.; Seidel, R. W.; Fischer, R. A. Cp* as a removable protecting group: low valent Zn (i) compounds by reductive elimination, protolytic and oxidative cleavage of Zn–Cp. *Dalton Trans.* **2013**, *42*, 10540-10544.
(26) (a) Jochmann, P.; Stephan, D. W. H_2 Cleavage, Hydride Formation, and Catalytic Hydrogenation of Imines with Zinc Complexes of C_5Me_5 and N-Heterocyclic Carbenes. *Angew. Chem. Int. Ed*. **2013**, *52*, 9831-9835. (b) Jochmann, P.; Stephan, D. W. Zincocene and Dizincocene N-Heterocyclic Carbene Complexes and Catalytic Hydrogenation of Imines and Ketones. *Chem. Eur. J.* **2014**, *20*, 8370-8378.
(27) Bollermann, T.; Gemel, C.; Fischer, R. A. Organozinc ligands in transition metal chemistry. *Coord. Chem. Rev.* **2012**, *256*, 537-555.
(28) (a) B. Fischer, J. Boersma, B. Kojić-Prodić, A. L. Spek, Reaction of bis(pentamethylcyclopentadienyl) zinc with bis (cyclo-octa-1,5-diene)nickel: crystal structure of $(C_5Me_5Ni)_2C_{16}H_{24}$. *J. Chem. Soc., Chem. Commun*. **1985**, 1237-1239. (b) Grirrane, A.; Resa, I.; Rodríguez, A.; Carmona, E.; Álvarez, E.; Gutierrez-Puebla, E.; Monge, A.; Galindo, A.; del Río, D.; Andersen, R. A. Zinc–Zinc Bonded Zincocene Structures. Synthesis and Characterization of $Zn_2(\eta^5\text{-}C_5Me_5)_2$ and $Zn_2(\eta^5\text{-}C_5Me_4Et)_2$. *J. Am. Chem. Soc.* **2007**, *129*, 693-703.
(29) (a) Zhu, Z.; Brynda, M.; Wright, R. J.; Fischer, R. C.; Merrill, W. A.; Rivard, E.; Wolf, R.; Fettinger, J. C.; Olmstead, M. M.; Power, P. P. Synthesis and Characterization of the Homologous M−M Bonded Series Ar 'MMAr'(M= Zn, Cd, or Hg; Ar'=C_6H_3-2,6-(C_6H_3-2,6-Pr^i_2)$_2$) and Related Arylmetal Halides and Hydride Species. *J. Am. Chem. Soc*. **2007**, *129*, 10847-10857. (b) Rit, A. Spaniol, T. P.; Maron, L.; Okuda, J. Molecular Zinc Dihydride Stabilized by N-Heterocyclic Carbenes. *Angew. Chem. Int. Ed.* **2013**, *52*, 4664-4667. (c) Roberts, A. J.; W. Clegg, W.; Kennedy, A. R.; Probert, M. R.; Robertson, S. D.; Hevia, E. Two alternative approaches to access mixed hydride-amido zinc complexes: synthetic, structural and solution implications. *Dalton Trans.* **2015**, *44*, 8169-8177. (d) Dawkins, M. J. C. Middleton, E.; Kefalidis, C. E.; Dange, D.; Juckel, M. M.; Maron, L.; Jones, C. Two-coordinate terminal zinc hydride complexes: synthesis, structure and preliminary reactivity studies. *Chem. Commun*. **2016**, *52*, 10490-10492.
(30) Fryzuk, M. D.; McConville, D. H.; Rettig, S. J. Reactions of the electron-rich binuclear hydride complexes [iso-$Pr_2P(CH_2)_xPPr\text{-}iso_2$] Rh]$_2$(μ-H)$_2$ (x = 2 or 3) with ZnR_2 and MgR'$_2$. *Organometallics* **1993**, *12*, 2152-2161.
(31) Riera, V.; Ruiz, M. A.; Tiripicchio, A.; Tiripicchio-Camellini, M. Manganese-Group 11 Element and -Zinc Mixed-Metal Clusters Derived from the Unsaturated Hydride $[Mn_2(\mu\text{-}H)_2(CO)_6(\mu\text{-tedip})]$ [tedip = $(EtO)_2POP(OEt)_2$]. X-ray Structures of $[Mn_2(\mu\text{-}AuPPh_3)(\mu\text{-}H)(CO)_6(\mu\text{-tedip})]$ and $[Mn_2\{\mu\text{-}Zn(N,N'\text{-}Me_2NCH_2CH_2NMe_2)\}(\mu\text{-}H)_2(CO)_6(\mu\text{-tedip})]$. *Organometallics* **1993**, *12*, 2962-2972.
(32) Bansemer, R. L.; Huffman, J. C.; Caulton, K. G. A bimetallic vanadium(I) polyhydride. *J. Am. Chem. Soc*. **1983**, *105*, 6163-6164.
(33) Cotton, F. A.; Murillo, L. A.; Walton, R. A. *Multiple Bonds Between Metal Atoms* **2005**, 3rd edition [F. A. Cotton, R. A. Walton, in 1st (**1981**) and 2nd (**1992**) ed.], Springer, New York.
(34) For $ZnPh_2$ preparation: Fleckenstein, J. E.; Koszinowski, K. Lithium organozincate complexes $LiRZnX_2$: common species in organozinc chemistry. *Organometallics* **2011**, *30*, 5018-5026.
(35) For $ZnCp^*_2$ and $Zn_2Cp^*_2$ preparation: Peloso, R.; Resa, I.; Rodríguez, A.; Carmona, E.; Freitag, K.; Jones, C.; Stasch, A.; Boutland, A. J.; Lips, F. in *Inorganic Syntheses*, **2018**, 33-45, P.P. Power (Ed.).
(36) Gil, D. M.; Echeverría, J.; Alvarez, S., The Tetramethylammonium Cation: Directionality and Covalency in its Interactions with Halide Ions. *submitted* **2022**.
(37) Carrasco, M.; Curado, N.; Maya, C.; Peloso, R.; Rodríguez, A.; Ruiz, E.; Alvarez, S.; Carmona, E., Interconversion of Quadruply and Quintuply Bonded Molybdenum Complexes by Reductive Elimination and Oxidative Addition of Dihydrogen. *Angew. Chem. Int. Ed.* **2013,** *52*, 3227-3231.
(38) Baratta, W.; Mealli, C.; Herdweck, E.; Ienco, A.; Mason, S. A.; Rigo, P., Nonclassical vs Classical Metal···H_3C–C Interactions: Accurate Characterization of a 14-Electron Ruthenium(II) System by Neutron Diffraction, Database Analysis, Solution Dynamics, and DFT Studies. *J. Am. Chem. Soc.* **2004,** *1236*, 5549-5562.
(39) Cole, J. M.; Gibson, V. C.; Howard, J. A. K.; McIntyre, G. J.; Walker, G. L. P., Multiple α-agostic interactions in a metal–methyl complex: the neutron structure of $[Mo(NC_6H_3Pr^i_2\text{-}2,6)_2Me_2]$. *Chem. Commun.* **1998**, 1829-1830.
(40) Bau, R.; Mason, S. A.; Parick, B. O.; Adams, C. S.; Sharp, W. B.; Legzdins, P., α-Agostic Interactions in $Cp^*W(NO)(CH_2CMe_3)_2$ and Related Nitrosyl Complexes. *Organometallics* **2001,** *20*, 4492-4501.